Developmental Cell, Volume *51*

Supplemental Information

Tricalbin-Mediated Contact Sites Control ER Curvature to Maintain Plasma Membrane Integrity

Javier Collado, Maria Kalemanov, Felix Campelo, Clélia Bourgoint, Ffion Thomas, Robbie Loewith, Antonio Martínez-Sánchez, Wolfgang Baumeister, Christopher J. Stefan, and Rubén Fernández-Busnadiego

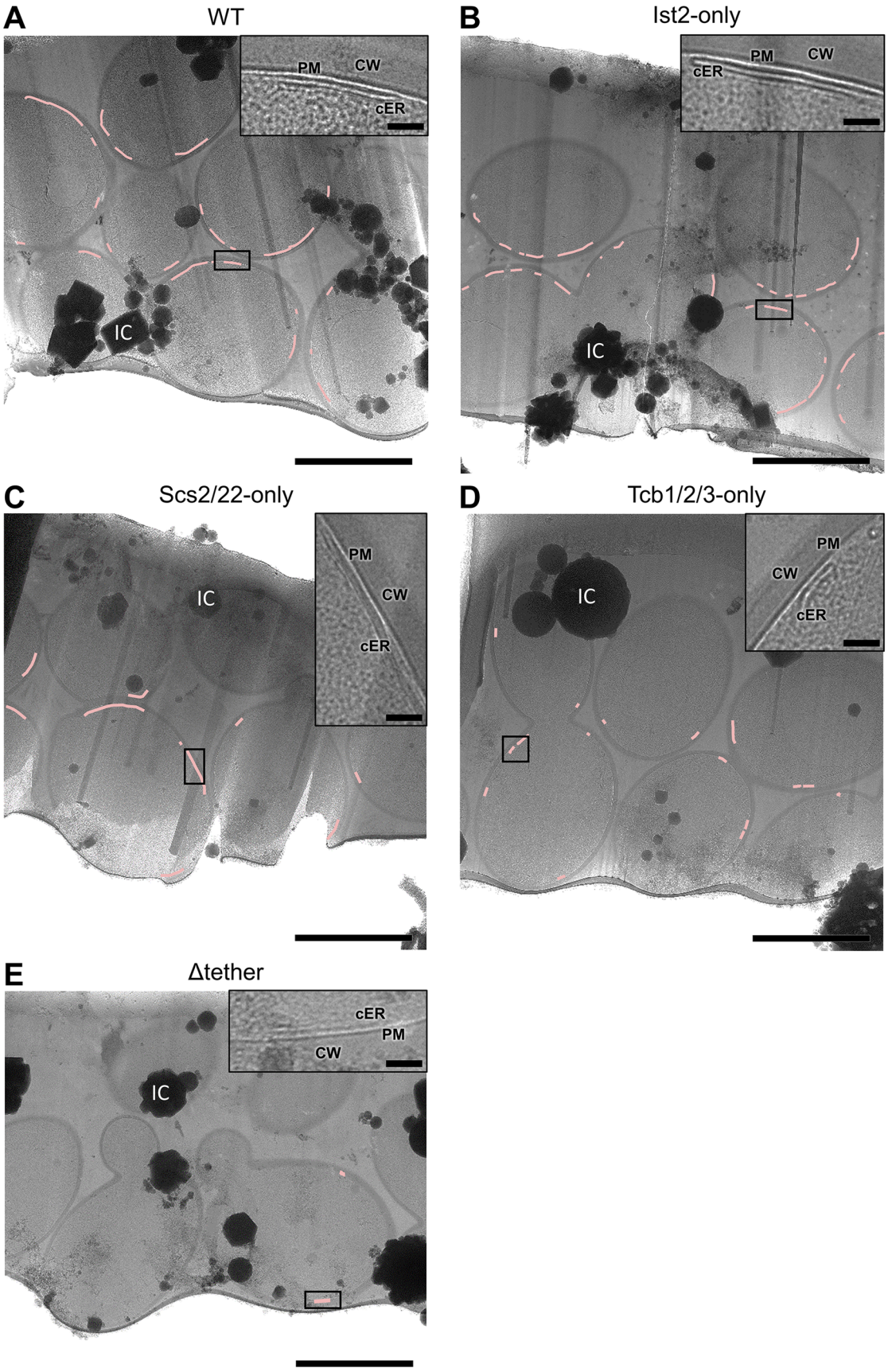
A
WT
PM
CW
cER
IC
B
Ist2-only
PM
CW
cER
IC
C
Scs2/22-only
IC
PM
CW
cER
D
Tcb1/2/3-only
IC
PM
CW
cER
E
Δtether
cER
PM
CW
IC

Figure S 1: Cryo-EM Overview Images of Cryo-FIB Lamellae. Related to Figure 2. Panels (A-E) show low magnification cryo-EM images of cryo-FIB lamellae milled through groups of cells. The profile of individual cells is marked by their cell wall. Pink lines mark cER (magnified in insets). CW: cell wall; cER: cortical ER; IC: ice crystal surface contamination; PM: plasma membrane. (**A**) WT cells, (**B**) Ist2-only cells, (**C**) Scs2/22-only cells, (**D**) Tcb1/2/3-only cells, (**E**) ∆tether cells. Scale bars: 3 µm (main panels), 500 nm (insets).

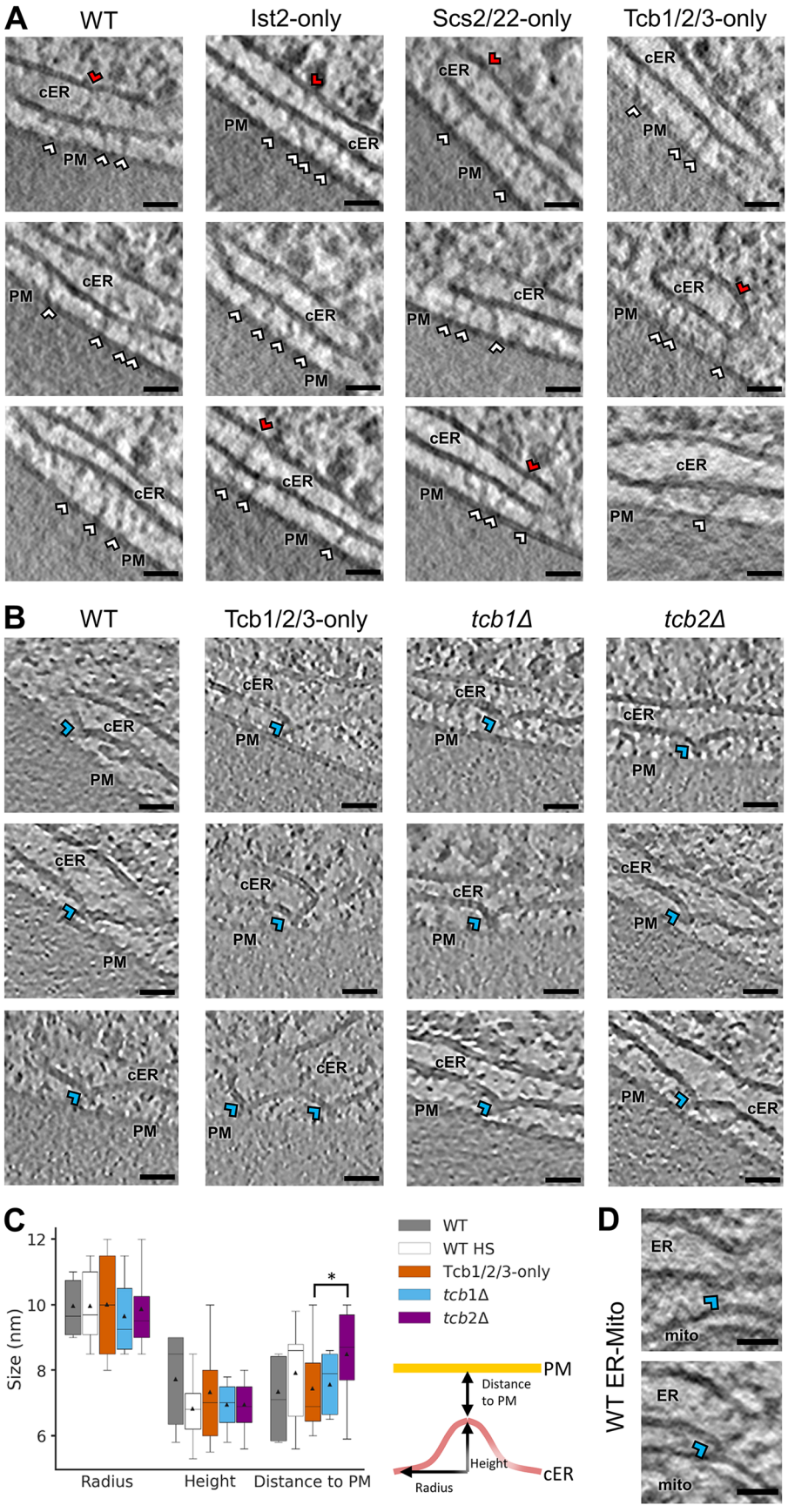
A
WT
Ist2-only
Scs2/22-only
Tcb1/2/3-only
cER
PM
B
WT
Tcb1/2/3-only
tcb1Δ
tcb2Δ
C
Size (nm)
12
10
8
6
Radius
Height
Distance to PM
*
WT
WT HS
Tcb1/2/3-only
tcb1Δ
tcb2Δ
PM
Distance to PM
Height
Radius
cER
D
WT ER-Mito
ER
mito

Figure S 2: High Magnification Images of ER-PM MCS. Related to Figure 1, Figure 2, Figure 4 and Figure 5. Gallery of magnified (**A**) tether structures and (**B**) cER peaks found in the different strains. White arrowheads: ER-PM tethers; red arrowheads: intraluminal cER tethers; blue arrowheads: cER peaks. cER: cortical ER; PM: plasma membrane. The images show 1.4 nm-thick tomographic slices. (**C**) Quantification of cER peak morphology in terms of radius, height and distance to the PM. All strains in which cER peaks were found are displayed except *tcb3Δ* + Tcb3-GFP. Boxes represent all measurements per strain: 6 (WT), 21 (WT HS), 24 (Tcb1/2/3-only), 7 (*tcb1*Δ) and 15 (*tcb2*Δ) cER peaks. The horizontal lines of each box represent 75% (top), 50% (middle) and 25% (bottom) of the values, whiskers 95% (top) and 5% (bottom), and a black triangle the average value. N = 6 (WT), 7 (WT HS), 16 (Tcb1/2/3-only), 5 (*tcb1*Δ) and 10 (*tcb2*Δ) cER-PM MCS (cER peak morphology was analyzed in 7 additional Tcb1/2/3-only and 5 *tcb2Δ* tomograms that were not used for other quantifications). * indicates $p < 0.05$ by unpaired t-test. (**D**) ER peaks (blue arrowheads) at ER-mitochondria MCS in WT cells. mito: mitochondrion. The contrast of the images in (A) and (D) was enhanced using a deconvolution filter. Scale bars: 25 nm.

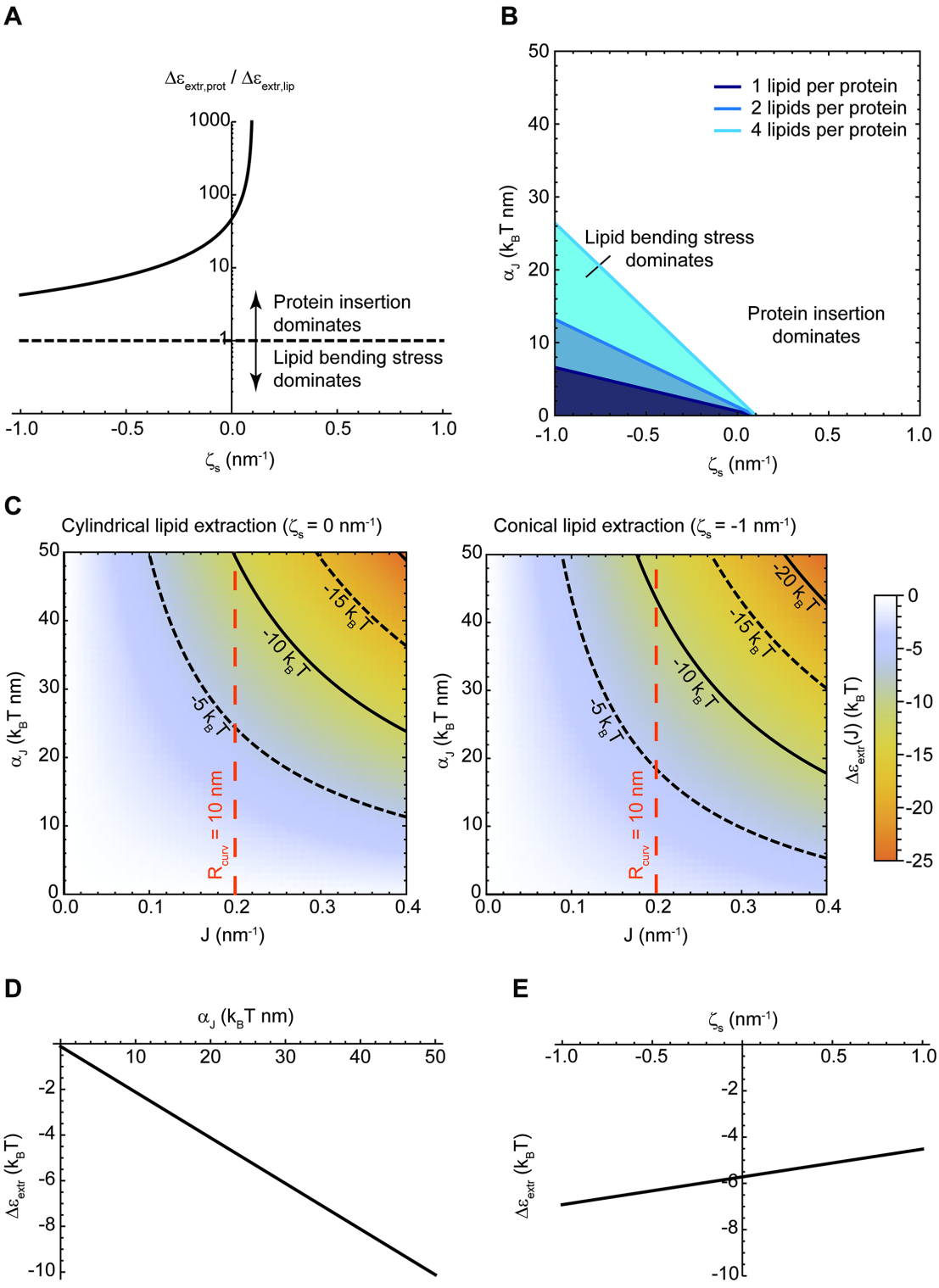

Figure S 3: Theoretical Model of How cER Peaks May Facilitate the Extraction of Lipids from the cER Membrane. Related to Figure 3 and STAR Methods. (**A**) Contribution of the protein insertion energy, $\Delta\varepsilon_{extr,prot}(J)$, to the total free energy change for lipid extraction relative to the elastic energy

relaxation of lipid extraction, $\Delta\varepsilon_{extr,lip}(J)$, for different values of the effective spontaneous curvature of the extracted lipids, ζ_s. When the relative contribution is larger than one, protein insertion energy dominates, whereas when the ratio is smaller than one, the elastic (bending) stress of the lipids dominates. (**B**) Transition line separating the regime of protein insertion domination (white region) from the regime of lipid bending stress domination (blue-shaded regions) for different values of the effective spontaneous curvature of the extracted lipids, ζ_s, and of the protein curvature sensitivity, α_J. The three lines correspond to the transition lines for extraction of 1, 2, or 4 lipids per protein (dark to light blue lines, see legend). (**C**) Energy barrier of lipid extraction from a curved membrane relative to a flat membrane (color code), $\Delta\varepsilon_{extr}(J)$, as a function of the total curvature of the membrane, J, and of the protein curvature sensitivity, α_J. (Left) Extraction of a cylindrical lipid with no effective spontaneous curvature, $\zeta_s = 0$. (Right) Extraction of a conical lipid with a large negative effective spontaneous curvature, $\zeta_s = -1\ nm^{-1}$. Isoenergy lines are plotted on both graphs (solid and dashed black lines), as well as a dashed red line marking the experimentally observed total curvature of the cER peaks. k_BT is the product of the Boltzmann constant and the absolute temperature. (**D**) Energy barrier for extraction of a cylindrical lipid ($\zeta_s = 0$) from a cER peak ($J = 0.2\ nm^{-1}$) relative to a flat membrane, $\Delta\varepsilon_{extr}$, as a function of the protein curvature sensitivity, α_J. (**E**) Energy barrier for lipid extraction from a cER peak ($J = 0.2\ nm^{-1}$) relative to a flat membrane, $\Delta\varepsilon_{extr}$, as a function of the effective spontaneous curvature of the extracted lipids, ζ_s, for the case of a lipid transfer protein with a curvature sensitivity, $\alpha_J = 28\ k_BT\ nm$.

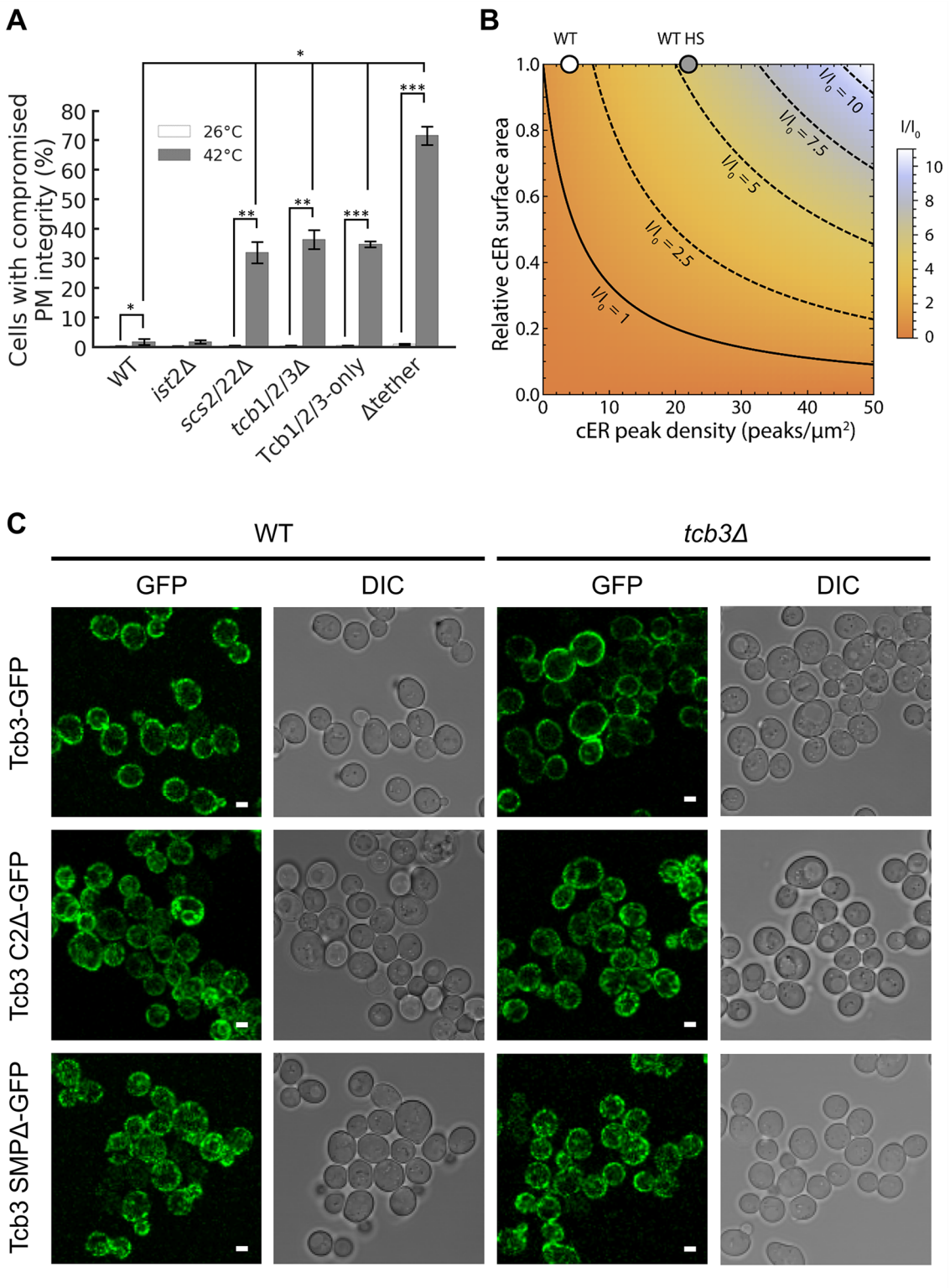

Figure S 4: PM Integrity Assays in Other Tether Mutants, Relative Contribution of cER Peaks and Flat Membranes to Lipid Transfer, and Localization of Tcb3 Truncations. Related to Figure 3, Figure 5, Figure 6 and STAR Methods. (**A**) PM integrity measurements of Ist2, Scs2/22, Tcb and

Δtether mutants upon 10 min incubation at 42 °C (right). The plot shows average values (white/grey bars) for each condition ± SE (error bars). *, ** and *** respectively indicate $p < 0.05$, $p < 0.01$ and $p < 0.001$ by Mann-Whitney-U test (for WT 42 °C data, which was not normally distributed) or unpaired t-test (for all other conditions). Four independent biological repeats were performed for all conditions. (**B**) Plot of I/I_0 (color coded), the lipid extraction current from cER peaks and flat parts of the cER membrane ($I=I_{peak} + I_{flat}$) relative the current from a completely flat membrane (I_0). The calculation was performed considering a 500 fold facilitation of lipid extraction by cER peak formation (Figure 3F) and modeling the peak as a conic structure of base radius of ~10 nm and height of ~7 nm (Figure S 2C). The X-axis shows the density of cER peaks, which is experimentally determined from cryo-ET data. The Y-axis shows the area of cER relative to WT, i.e. = 1 for WT cells and < 1 for conditions with reduced total levels of cER (e.g. Tcb1/2/3-only). The graph shows that for WT cells, the lipid flows from cER peaks and flat membranes are roughly equivalent ($I/I_0 \approx 1.8$; white circle). However, lipid flow from cER peaks dominates in heat-shocked WT cells (WT HS) due to the observed ~6-fold increase in cER peak density ($I/I_0 \approx 5.4$; grey circle). Note that increasing cER peak density can only substantially increase I/I_0 when total levels of cER are high. (**C**) Light microscopy imaging by GFP fluorescence (mid-section confocal images; left) and DIC (right) of WT and *tcb3Δ* cells expressing the following constructs: full length Tcb3-GFP, Tcb3 C2Δ-GFP and Tcb3 SMPΔ-GFP. Scale bars: 2 µm.

Condition	Number of experiments	Number of MCS	Total number of intermembrane distance measurements	Total number of cER thickness measurements	Total number of cER curvature measurements	Total cER area analyzed (μm²)
WT	2	6	685,160	531,487	2,612,817	1.7
WT HS	2	7	-	-	-	1.7
Ist2-only	2	5	663,763	525,115	2,327,393	1.5
Scs2/22-only	2	5	478,590	388,246	1,824,833	1.1
Tcb1/2/3-only	3	9	552,956	368,510	2,053,182	1.3
Δtether	1	4	-	-	-	0.16
tcb1Δ	2	5	-	-	-	0.9
tcb2Δ	2	5	-	-	-	0.7
tcb3Δ	2	5	-	-	-	0.8
tcb1/2Δ	2	5	-	-	-	0.8
tcb1/2/3Δ	2	5	-	-	-	1.4
tcb1/2/3Δ HS	2	5	-	-	-	0.7
tcb3Δ + Tcb3-GFP HS	2	3	-	-	-	0.3
tcb3Δ + Tcb3-SMPΔ-GFP HS	2	3	-	-	-	0.4
tcb3Δ + Tcb3-C2Δ-GFP HS	2	3	-	-	-	0.4
ER-Mito	3	5	81,124	-	-	-
Nuc-Vac	2	5	362,899	-	-	-

Table S 1: Statistics of Cryo-ET Experiments. Related to Figure 1, Figure 2, Figure 3, Figure 4, Figure 5 and Figure 6. The column “Number of MCS” refers to ER-PM MCS in all cases except ER-mitochondria (ER-Mito) and nucleus-vacuole (Nuc-Vac) MCS. In the following columns, “total” indicates aggregated values for all tomograms analyzed in each condition. The total number of intermembrane distance measurements reflects the number of triangles from the first membrane (PM in ER-PM MCS, mitochondria in ER-mitochondria MCS, vacuole in nucleus-vacuole MCS) from which normal vectors

intersected the second membrane. The total number of cER thickness measurements reflects the number of triangles from the PM from which normal vectors intersected the cER membrane twice. The total number of cER curvature measurements reflects the number of triangles of the cER membrane. The total cER area analyzed is the sum of the area of all cER triangles. For the calculation of cER peak density, the number of cER peaks per condition was divided by half of the total cER area, as cER peaks were only found on the side of the cER membrane facing the PM. For simplicity, values are only shown for the conditions plotted (Figure 1E, Figure 2G, H, I, Figure 3E and Figure 6D).